Childs Nerv Syst (2012) 28:273–282
DOI 10.1007/s00381-011-1604-9

ORIGINAL PAPER

Epileptogenic brain lesions in children: the added-value of combined diffusion imaging and proton MR spectroscopy to the presurgical differential diagnosis

Slim Fellah · Virginie Callot · Patrick Viout · Sylviane Confort-Gouny · Didier Scavarda · Philippe Dory-Lautrec · Dominique Figarella-Branger · Patrick J. Cozzone · Nadine Girard

Received: 8 July 2011 / Accepted: 28 September 2011 / Published online: 27 October 2011

Abstract
Purpose Focal cortical dysplasia (FCD), dysembryoplastic neuroepithelial tumors (DNTs), and gangliogliomas (GGs) share many clinical features, and the presurgical differential diagnosis of these lesions using conventional magnetic resonance imaging (MRI) is challenging in some cases. The purpose of this work was thus to evaluate the capacity of diffusion-weighted imaging (DWI) and proton magnetic resonance spectroscopy (MRS) to distinguish each lesion from the others.
Methods Seventeen children (mean age 9.0±4.7 years), who had been referred for epilepsy associated with a brain tumor and operated, were selected. Preoperative MRI examinations were performed on a 1.5 T system and included anatomical images [T2-weighted, fluid-attenuated inversion recovery (FLAIR) and T1 pre- and post-injection images] as well as DWI and MRS [echo time (TE) = 30 and 135 ms]. Apparent diffusion coefficient (ADC) values were calculated in the lesion and healthy control. MRS relative quantification consisted in normalizing each metabolite by the sum (S) of all metabolites ($S_{TE=135\ ms}$ = NAA+Cr+Cho; $S_{TE=30\ ms}$ = NAA+Cr+Cho+Glx+mI). Univariate and multivariate analyses were performed in order to determine which criteria could differentiate the different epileptogenic brain lesions.
Results When taken alone, none of the MRI parameters was able to distinguish each disease from the others. Conventional MRI failed classifying two patients. When adding ADC to the linear discriminant analysis (LDA), one patient was still misclassified. Complete separation of the three groups was possible when combining conventional MRI, diffusion, and MRS either at long or short TE.
Conclusion This study shows the added-value of multimodal MRI and MRS in the presurgical diagnosis of epileptogenic brain lesions in children.

Keywords Focal cortical dysplasia · Dysembryoplastic neuroepithelial tumors · Intracranial gangliogliomas · Diffusion MRI · MR spectroscopy · Child

S. Fellah (✉) · V. Callot · P. Viout · S. Confort-Gouny · P. J. Cozzone · N. Girard
Centre de Résonance Magnétique Biologique et Médicale (CRMBM), Aix-Marseille Univ and CNRS, Marseille, France
e-mail: slim.fellah@univmed.fr

D. Scavarda
Département de neurochirurgie pédiatrique, Aix-Marseille Univ and APHM, Hôpital de la Timone, Marseille, France

P. Dory-Lautrec · N. Girard
Service de Neuroradiologie Diagnostique et Interventionnelle, Aix-Marseille Univ and APHM, Hôpital de la Timone, Marseille, France

D. Figarella-Branger
Service d'Anatomie Pathologique et de Neuropathologie, Aix-Marseille Univ and APHM, Hôpital de la Timone, Marseille, France

Introduction

Focal cortical dysplasia (FCD), dysembryoplastic neuroepithelial tumors (DNTs) and gangliogliomas (GGs) are the most common brain lesions encountered in pediatric epilepsy [5, 10, 16, 25]. Complete resection of the lesion can be a good remedy for intractable epilepsy in carefully selected patients [1, 14, 19, 22, 25]. However, treatment policy differs between these diseases, and most surgical

decisions, including the selection of surgical candidates, determination of when to operate, and outcome expectation, depend heavily on the preoperative diagnosis. In the case of FCD and DNTs which are supposed to be non-progressive lesions with an excellent long-term outcome, surgery can be performed after a long period of seizure manifestations. In contrast, GGs, which are associated with a more aggressive astroglial component, must be operated more quickly to avoid evolution into anaplastic GG (grade III of the WHO classification [17]) or even into glioblastoma (grade IV) [6, 12, 18]. It is therefore of the utmost importance to distinguish these brain lesions from each other. However, although these lesions are generally different in their pathological characteristics, the clinical and imaging features can be similar in some cases (Fig. 1) and clear identification of the lesion type may be confusing. Conventional magnetic resonance imaging (MRI) plays a key role in the field of preoperative diagnosis [7, 23, 24, 27] in epilepsy surgery, but in some cases, it is still insufficient. The purpose of this work is thus to investigate other MRI methods that may help differentiating epileptogenic lesions such as DNTs, FCD, and GGs.

Diffusion-weighted imaging (DWI), perfusion-weighted imaging (PWI), and magnetic resonance spectroscopy (MRS), which provide structural, hemodynamic, and metabolic information, respectively, are among the techniques of interest. Some of these methods have been investigated in order to characterize epileptogenic tumors [4, 31, 34, 35] and, in particular, DNTs. However, to the best of our knowledge, no study specifically dedicated to the differential diagnosis of epileptogenic lesions using DWI, PWI, and MRS in a children population has been reported so far.

The goal of this study of 20 children with epileptogenic brain lesions was to evaluate the capacity of DWI, PWI, and proton MRS to distinguish DNTs from FCD, GGs, and other epileptogenic tumors.

Patients and methods

Patients

Between 2004 and 2010, we retrospectively selected all children who had been referred for epilepsy associated with a brain tumor. From the 51 patients who fulfilled these criteria, we selected all those who had been operated. Overall, 20 children (7 females, 13 males; age range 1 month to 16 years, mean 9±4.7 years) met the above

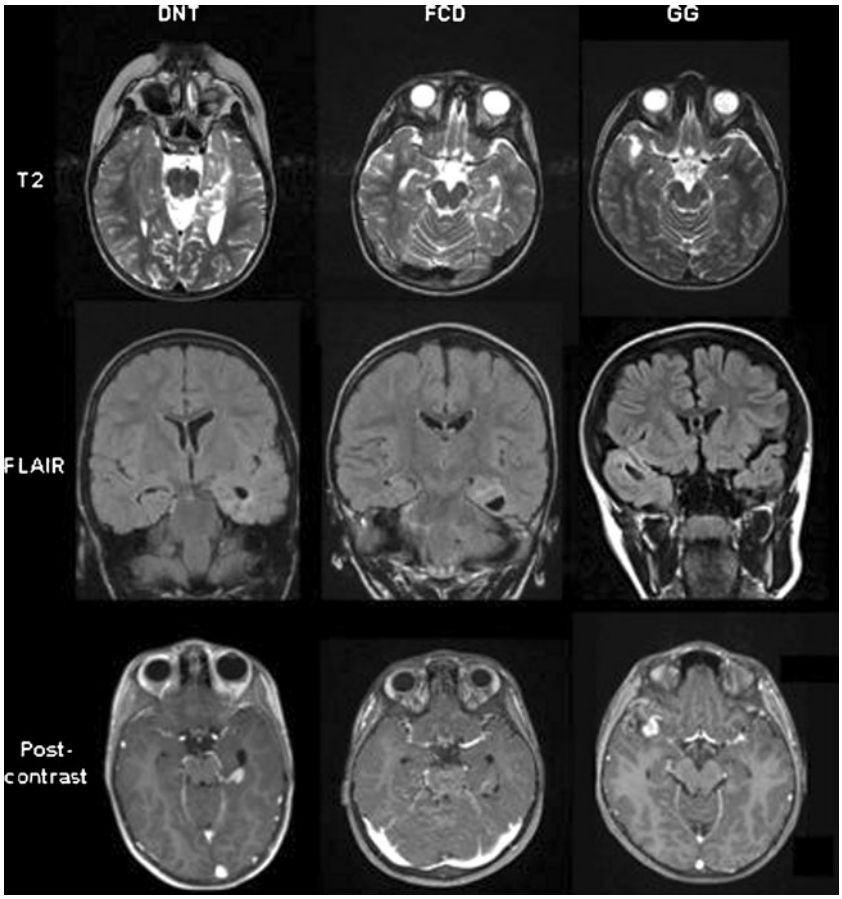

Fig. 1 Example of confounding diagnosis based on conventional MRI. The three types of lesions present cysts on T2-weighted images; no edema was found on FLAIR images, and CE was present in DNT and GG

criteria and were included in this study. This patient's population included five FCD, eight DNTs, four GGs, one pilocytic astrocytoma (PA), one oligoastrocytoma (OA), and one ependymoma (E). The duration of epilepsy varied from 2 months to 10 years (mean 2.4±2.6 years), and the age at onset varied from 10 days to 14 years (mean 6.4±4.1 years).

Magnetic resonance imaging

All MRI examinations were performed on a 1.5 T system (Symphony Siemens, Erlangen, Germany). Imaging protocol included a standard gradient-echo T1 sequence in the sagittal plane [repetition time (TR) = 359 ms, echo time (TE) = 4.48 ms], slice thickness = 4 mm, field of view (FOV) = 300 mm total acquisition time = 1 min 29 s), an axial turbo spin-echo T2 (TR = 5,200 ms, TE = 148 ms, slice thickness = 3 mm, FOV = 240 mm, total acquisition time = 3 min 28 s) and a coronal fluid-attenuated inversion recovery (FLAIR) images (TR = 10,000 ms, TE = 108 ms, slice thickness = 3 mm, FOV = 230 mm, total acquisition time = 4 min). DWI and MRS were performed before gadolinium administration, while PWI and 3D gradient echo T1 sequence (TR = 2,060 ms, TE = 2.79 ms, slice thickness = 0.8 mm, FOV = 256 mm, total acquisition time = 5 min 40 s) were acquired during and after.

Diffusion-weighted image

DWIs were obtained using an axial, multi-slice echo-planar spin-echo sequence (TR = 3,500 ms, TE = 101 ms, slice thickness = 5 mm, three averages per image, FOV = 334 mm, total acquisition time = 1 min 50 s). Diffusion was measured in three orthogonal directions at two *b*-values (500 and 1,000 $s mm^{-2}$). An additional set of images was obtained with no diffusion weighting ($b=0$ $s mm^{-2}$). Apparent diffusion coefficient (ADC) maps were calculated on a pixel-by-pixel basis.

Proton MRS

A single voxel technique was performed with a voxel of interest (VOI) of 8 cm^3 (20×20×20 mm) centered in the bulk of the tumor, away from the scalp (to avoid lipid contamination) and the temporal bone. Spectra were acquired by Point Resolved Spectroscopy (PRESS) acquisition with short (30 ms) and long (135 ms) TE (TR = 1,500 ms, 50 scans, total acquisition time of 1 min 21 s for each sequence). When possible, water (H_20) signal has also been acquired.

Perfusion-weighted imaging

Dynamic susceptibility contrast T2*-weighted echo-planar gradient-echo images were acquired in 13 patients (TR = 1,480 ms, TE = 30 ms, flip angle 90°, no gap, slice thickness = 5 mm, FOV = 281 mm, 50 sets of 20 images, total acquisition time = 1 min 21 s). A single standard dose of 0.1 mmol/kg of body weight (Dotarem, Guerbet, France) was rapidly administrated intravenously through a power injector at 2– 5 ml s^{-1} depending on weight and age of the patient.

Post-processing and data analysis

Two investigators evaluated the MR images by consensus. Lesion location, calcifications, edema, contrast enhancement (CE), cystic component, hemorrhage, mass effect, and lesion shape were recorded. As shown in Table 1, CE, cysts, and lesion shape were coded using a score from 1 to 4 while edema was binary-coded.

MRS relative quantification consisted in normalizing each metabolite by the sum (S) of all metabolites analyzed (TE = 135 ms, sum = NAA+Cr+Cho; TE = 30 ms, sum = NAA+Cr+Cho+Glx+mI). The metabolite ratios Cho/NAA, Cho/Cr, lip/S, and mI/Cr were also calculated. Metabolite values were not normalized to H_2O signal since data was only available for 15 out of the 20 patients included in this study. Post-processing of the MR spectroscopy data was carried out using the AMARES-MRUI FORTRAN code [28] included in a homemade software developed under Interactive Data Language (IDL) environment (Research System, Boulder, CO, USA). *N*-acetylaspartate (NAA) at 2.02 ppm, choline-containing components (Cho) at 3.22 ppm, creatine, and phosphocreatine (Cr) at 3.03 ppm were identified on the long and short echo-time spectrum. In addition, myoinositol (mI) at 3.56 ppm, lipids (lip) at 0.85 and 1.70 ppm, and the complex glutamine–glutamate (Glx) at 2.16 and 2.28 ppm were recognized on the MR spectrum at short TE.

Post-processing of perfusion data was done using Perfscape and Neuroscape softwares (OLEA medical, SAS, La Ciotat, France). Cerebral blood flow (CBF), corrected cerebral blood volume (CBV), time to peak (TTP), mean transition time (MTT), and permeability index (K2) maps were generated after verification of an automatically detected arterial input function (AIF). In PWI and DWI, all regions of interest (ROIs) were drawn by consensus for the

Table 1 Coding scores of conventional MRI parameters for statistical analysis

	Score 1	Score 2	Score 3	Score 4
Lesion shape	Rectangular	Triangular	Round	Undefined
Cysts	Absent	1 cyst	Microcysts	Multiple cysts
CE	Absent	Nodular	Homogeneous	Heterogeneous
Edema	Absent	Present		

recording of ADC and perfusion parameters. Tumor ROI was manually placed on CE region, when existing, avoiding macroscopic cysts, cerebrospinal fluid, and major vessels. In case of non-enhancing lesions, tumor ROI was placed in the area with lowest ADC and/or highest CBV value. Normal-appearing mirrored ROIs were used to obtain control values. All perfusion parameters (CBF, CBV, MTT, TTP, and K2) were then normalized by dividing tumoral values by the normal contralateral value to obtain relative ratios (rCBF, rCBV, rMTT, rTTP, and rK2, respectively).

Statistical analysis

Seventeen patients were included in the statistical analysis and were classified into three pathologic diagnosis groups: FCD, DNT, and GG. PA, OA, and E groups were excluded due to the insufficient number of patients. The JMP 5 software (SAS Institute, Cary, NC, USA) was used for the analyses. Data were analyzed with univariate and multivariate statistical analysis. Univariate statistical analysis was performed with multiple parameters from DWI and MRS to determine which criteria were significantly different among groups. Univariate analysis could not be performed on perfusion data because of the small number of patients having PWI. The nonparametric Wilcoxon test was performed to compare the distribution of these parameters among the groups. When this test yielded significant result, we also performed a Tukey–Kramer test. Multivariate linear discriminant analysis (LDA) was used combining all MRI and MRS parameters to differentiate the groups. Significance was set at a p value less than 0.05.

Results

Clinical and neuroradiological findings

Results with data from lesion location, edema, CE, cysts, hemorrhage, lesion shape, age at onset, and duration of epilepsy are presented in Table 2. Among the 20 patients, three were still presenting seizures after surgery but at a lower frequency than before surgery. The majority of the lesions were found to be located in the temporal lobe (14 patients) followed by the frontal lobe (four patients), the occipital lobe (one patient), and the parieto-occipital lobe (one patient). Our results showed that edema was detected on FLAIR images in two patients histopathologically diagnosed as GG and pilocitic astrocytoma. CE was identified in 13 patients (65%) on post-contrast T1-weighted images. We noted that all the GGs presented a CE while all FCDs did not enhance after gadolinium injection. Six DNTs (75%) exhibited CE as nodular in four and heterogeneous enhancement in two. All but one DNT presented a cystic appearance. Six had multiple/microcysts and only one DNT showed one cyst. Only one patient presented hemorrhage (DNT), and neither mass effect nor calcifications were found in the studied population. Univariate analysis showed that GGs could be distinguished from FCDs and from DNTs by CE ($p<0.05$), and DNTs could be differentiated from FCDs by cysts criterion ($p<0.05$). None of the other neuroradiological criteria was able to differentiate the three groups from each other ($p>0.05$).

Diffusion, perfusion, and spectroscopy findings

Diffusion and spectroscopy data were available in all patients, while perfusion MRI was performed in ten patients among the 17 included in the statistical analysis. Table 3 resumes quantitative data from DWI, PWI, and MRS for each group. Univariate analysis revealed that DNT patients had the highest ADC values and were significantly different from those of FCD and GG patients ($p<0.05$; Fig. 2a). The MRS quantitative analysis demonstrated a significant difference in Cr/S and Cho/Cr ratios at long TE between FCD and GG groups (Cr/S ratio was higher in FCDs, while Cho/Cr ratio was higher in GGs; $p<0.05$; Fig. 2c and d). At short TE, the Cho/S ratio was significantly higher in GGs compared to DNTs ($p<0.05$; Fig. 2b). Univariate statistical analysis could not be performed on perfusion parameters (rCBF, rCBV, rMTT, rTTP, and rK2) because of the small proportion of patients having PWI data.

Multivariate analysis

LDA was performed on the17 children included in the statistical analysis. The three groups (FCD, DNT, and GG) could not be separated correctly with conventional MRI (including T1- and T2-weighted, FLAIR, and post-contrast T1-weighted images), long TE MRS, and short TE MRS taken separately with a number of misclassified patients of two (Fig. 3a), seven, and six, respectively. Variables and combination of variables were tested and incremented in the analysis. Thus, when combining conventional MRI with ADC, one patient was still misclassified (Fig. 3b). Complete separation of the three lesion types was obtained with the combination of conventional MRI scores, ADC, and long TE MRS (Fig. 4a). Moreover, a more accurate result was obtained by combining conventional MRI scores, ADC, and short TE MRS (Fig. 4b). However, when performing LDA with conventional MRI, ADC, long and short MRS data, we found no significant supply compared to the previous combinations (Fig. 4c). Thus, if available scan time is reduced, MRS data at short TE should be acquired preferably. Table 4 resumes the sensitivity and specificity values of each technique or combination of techniques for each group of lesion.

Table 2 Clinical and conventional MRI features for each patient

Patient (no.)	Age	Sex	Pathological data	Location	Edema	CE	Cysts	Hemorrhage	Lesion shape	Age at onset	Duration of epilepsy
1	11 years	M	DNT	L-temporal	−	Nodular	Multicysts	−	Rectangular	6 years	5 years
2	2 years	F	DNT	R-temporal	−	Nodular	1 cyst	−	Rectangular	1 year	1 year
3	12 years	M	DNT	Temporopolar	−	Heterogeneous	−	−	Triangular	10 years	2 years
4	13 years	F	DNT	L-temporal	−	−	Microcysts	−	Triangular	11 years	2 years
5	8 years	M	DNT	L-occipital	−	Nodular	Multicysts	+	Triangular	7 years	5 months
6	4 years	F	DNT	L-temporomesial	−	Heterogeneous	Microcysts	−	Undefined	10 days	4 years
7	13 years	M	DNT	R-temporal	−	Nodular	Microcysts	−	Round	12 years	4 months
8	14 years	F	DNT	R-temporal	−	−	Multicysts	−	Round	9 years	5 years
9	6 years	M	FCD	R-temporal	−	−	−	−	Undefined	5 years	1 year
10	10 years	M	FCD	L-temporal	−	−	1 cyst	−	Triangular	9 years	1 year
11	6 years	F	FCD	L-temporomesial	−	−	1 cyst	−	Triangular	4 years	2 years
12	14 years	F	FCD	R-frontal	−	−	−	−	Undefined	4 years	10 years
13	4 years	M	FCD	R-frontal	−	−	−	−	Undefined	10 days	4 months
14	16 years	M	GG	R-frontal	−	Homogeneous	Microcysts	−	Triangular	14 years	8 months
15	10 years	M	GG	R-temporal	−	Heterogeneous	Multicysts	−	Round	8 years	2 years
16	15 years	M	GG	R-temporal	−	Heterogeneous	1 cyst	−	Round	6 years	8 years
17	6 years	M	GG	L-frontal	+	Heterogeneous	1 cyst	−	Round	4 years	2 years
18	11 years	M	PA	L-temporal	+	Heterogeneous	Multicysts	−	Round	8 years	2 months
19	2 months	M	OA	R-temporal	−	Heterogeneous	−	−	Round	10 days	2 months
20	11 years	F	E	R-parietooccipital	−	Nodular	Microcysts	−	Round	9 years	1 year

CE contrast enhancement, *DNT* dysembruoplastic neuroepithelial tumor, *E* ependymoma, *F* female, *FCD* focal cortical dysplasia, *GG* ganglioglioma, *L* left, *M* male, *OA* oligoastrocytoma II, *PA* pilocitic astrocytoma I, *R* right, + present, − absent

Table 3 Diffusion, perfusion and MR spectroscopy quantitative data obtained in each lesion group

Parameter	DNT (*n*=8)		FCD (*n*=5)		GG (*n*=4)		PA (*n*=1)	OA (*n*=1)	E (*n*=1)
	Range	Mean (SD)	Range	Mean (SD)	Range	Mean (SD)			
ADC (10–3 mm s^{-2})	1.18–2.14	1.62 (0.34)	0.92–1.18	1.05 (0.12)	0.78–1.33	1.04 (0.24)	1.05	0.68	1.11
rADC	1.35–2.66	1.85 (0.46)	0.95–1.48	1.15 (0.20)	0.99–1.74	1.38 (0.38)	1.12	0.70	1.27
NAA/S (TE 135)	0.21–0.47	0.35 (0.10)	0.18–0.39	0.30 (0.08)	0.28–0.48	0.38 (0.08)	0.20	0.26	0.25
Cr/S (TE 135)	0.22–0.35	0.27 (0.04)	0.26–0.44	0.32 (0.07)	0.18–0.23	0.21 (0.02)	0.14	0.22	0.36
Cho/S (TE 135)	0.19–0.51	0.38 (0.11)	0.33–0.46	0.39 (0.06)	0.33–0.50	0.42 (0.08)	0.66	0.52	0.39
Cho/Cr (TE 135)	0.55–2.01	1.47 (0.44)	0.87–1.74	1.28 (0.36)	1.30–2.74	2.02 (0.45)	4.64	2.36	1.09
Cho/NAA (TE 135)	0.42–2.23	1.28 (0.68)	0.86–2.16	1.42 (0.53)	0.67–1.77	1.19 (0.48)	3.28	1.97	1.61
NAA/S (TE 30)	0.11–0.27	0.17 (0.05)	0.10–0.21	0.16 (0.04)	0.15–0.33	0.24 (0.08)	0.28	0.11	0.12
Cr/S (TE 30)	0.04–0.20	0.15 (0.06)	0.14–0.19	0.17 (0.02)	0.13–0.24	0.18 (0.05)	0.17	0.16	0.14
Cho/S (TE 30)	0.07–0.20	0.16 (0.04)	0.12–0.23	0.16 (0.04)	0.19–0.32	0.23 (0.06)	0.32	0.18	0.14
mI/S (TE 30)	0.08–0.26	0.13 (0.06)	0.07–0.23	0.15 (0.07)	0.03–0.08	0.06 (0.02)	0.18	0.08	0.21
Glx/S (TE 30)	0.35–0.68	0.48 (0.13)	0.31–0.46	0.36 (0.06)	0.34–0.68	0.46 (0.15)	0.72	0.47	0.38
lip/S (TE 30)	0.23–1.26	0.49 (0.36)	0.30–0.64	0.43 (0.15)	0.34–1.02	0.67 (0.28)	1.55	0.16	0.41
Cho/Cr (TE 30)	0.75–1.64	1.15 (0.33)	0.62–1.23	0.95 (0.22)	1.12–1.87	1.36 (0.30)	1.87	1.14	0.97
Cho/NAA (TE 30)	0.55–1.53	0.98 (0.35)	0.90–1.13	1.00 (0.11)	0.72–1.29	1.03 (0.25)	1.16	1.61	1.11
mI/Cr (TE 30)	0.43–2.08	0.99 (0.56)	0.35–1.21	0.87 (0.36)	0.20–0.39	0.32 (0.08)	1.05	0.52	1.50
	DNT (*n*=6)		FCD (*n*=2)		GG (*n*=2)		PA (*n*=1)	OA (n=1)	E (*n*=1)
rCBF	0.48–2.90	1.08 (0.90)	0.91–2.03	1.47 (0.79)	1.68–4.36	3.02 (1.89)	0.74	2.65	3.05
rCBV	0.50–3.05	1.08 (0.98)	0.77–1.82	1.29 (0.74)	1.15–4.36	2.75 (2.27)	0.93	2.11	2.38
rMTT	0.00–0.81	0.25 (0.34)	0.33–0.69	0.51 (0.25)	0.17–2.60	1.38 (1.71)	0.00	0.14	0.73
rTTP	0.79–1.05	0.93 (0.08)	0.84–1.03	0.94 (0.14)	0.97–1.00	0.99 (0.02)	0.96	0.95	1.01
rK2	0.93–19.15	5.52 (7.09)	0.91–4.10	2.51 (2.25)	11.65–85.02	48.33 (51.89)	13.96	3.55	6.17

ADC Apparent diffusion coefficient, *Cho* choline-containing components, *Cr* creatine, *DNT* dysembruoplastic neuroepithelial tumor, *E* ependymoma, *FCD* focal cortical dysplasia, *GG* ganglioglioma, *Glx* glutamine–glutamate complex, *lip* lipids, *mI* myoinositol, *NAA* *N*-acetyl aspartate, *OA* oligoastrocytoma II, *PA* pilocitic astrocytoma I, *rADC* relative ADC, *rCBF* relative cerebral blood flow, *rCBV* relative cerebral blood volume, *rK2* relative permeability index, *rMTT* relative mean transit time, *rTTP* relative time to peak, *S* sum of all metabolites, *TE* time echo

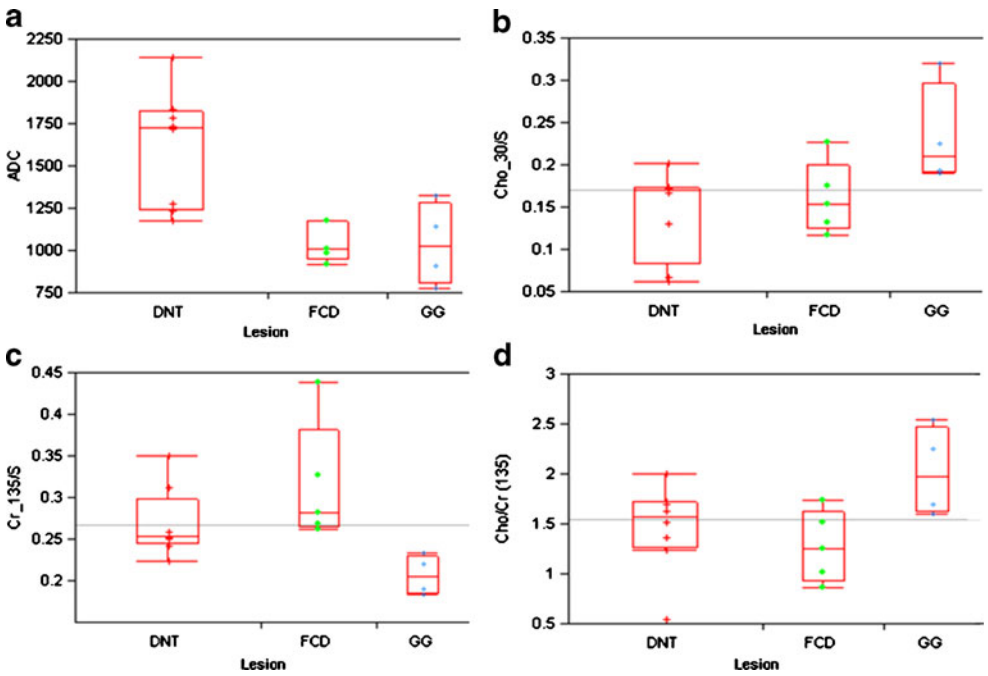

Fig. 2 Univariate analysis with different MR parameters in DNT, FCD, and GG groups. Significantly higher ADC was found in DNTs compared to FCD and GGs ($p<0.05$) (**a**). GG group had the highest Cho/S ratio at short TE and was significantly different from DNT ($p<0.05$) (**b**). At long TE, significant difference was found between FCD and GG groups ($p<0.05$): FCD showed high Cr/S ratio (**c**), while the highest Cho/Cr ratio was observed in GG (**d**)

Discussion

Presurgical diagnosis of epileptogenic brain tumors in children is important for treatment planning. However, it is still challenging in some cases despite the considerable contribution of all neuroimaging techniques. Indeed, some authors have shown that no hallmark specific to either DNT, FCD, or GG on preoperative MRI could differentiate the three types before surgery [24, 27]. Others have acknowledged the possibility of misdiagnosing DNTs and GGs as OA, oligodendroglioma, and astrocytoma [11]. In this relatively large MRI study on child patients with epileptogenic brain tumors, we have shown, for the first time, the promising potential of multimodal MRI as a presurgical diagnosis tool. Our neuroradiological findings in DNTs, GGs, and FCD were mostly similar to the literature [5, 7, 12, 15, 23, 24, 27, 29, 33]. The temporal lobe was the most frequent location for these lesions. Low signal on T1-weighted images and high intensity signal on T2-weighted and FLAIR images were usually observed. Edema was generally absent in the three types of lesions, while CE was common but variably appreciated. Indeed, CE in DNTs was reported to be low in the literature [1, 4, 24], but it can vary from 18% [4] to 50% [23] of the cases. GGs usually show CE [12, 20, 29, 36], but when located in mesial temporal lobe, they tend to show no CE. However, although FCD commonly lacks CE on post-gadolinium T1-weighted images, some exceptions have been reported [2, 15, 30].

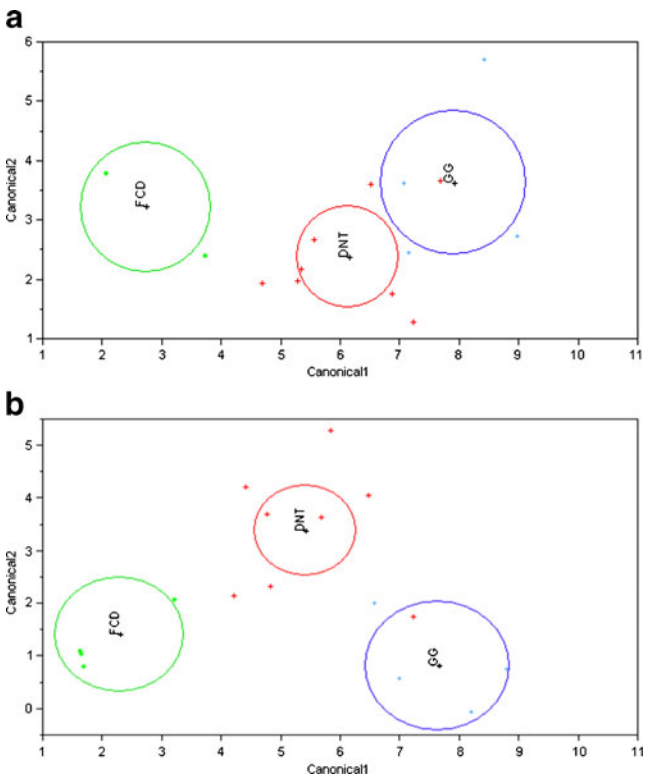

Fig. 3 LDA showing two misclassified patients with conventional MRI (**a**) and one misclassified patient when adding ADC to the analysis (**b**)

In this study, we found that the DNTs had significantly higher ADC values than FCD and GGs, as previously reported in a retrospective study of 275 children and adults patients with various brain tumors [34]. Moreover, ADC values in DNT patients have been shown to be significantly higher compared to a control group in a study with adult and children population [4]. It is also known from an adult study that DNTs display the highest ADC values among the benign tumors and that ADC could help in grading tumors

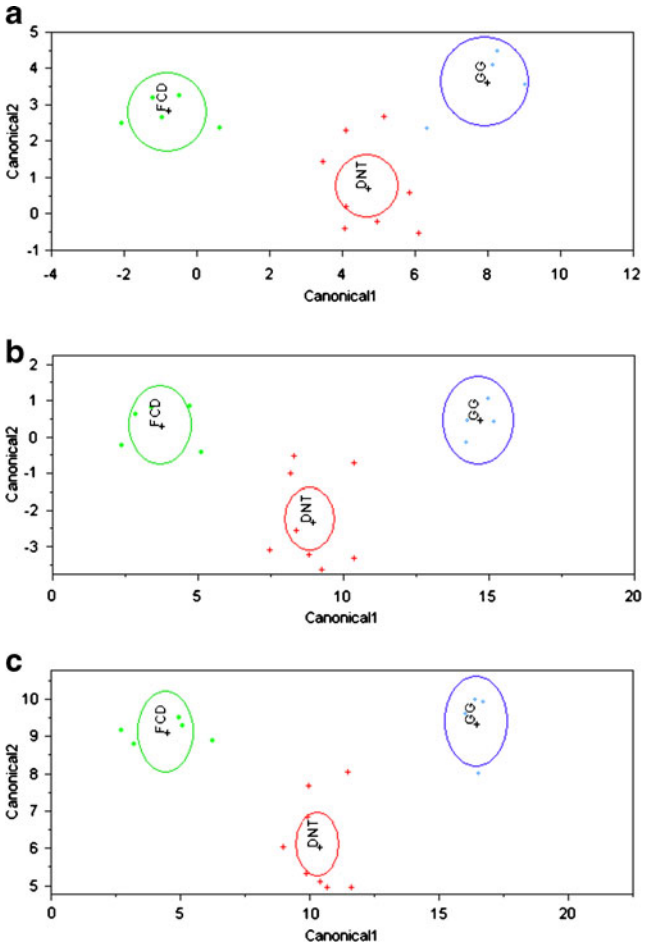

Fig. 4 LDA showing complete separation of the three groups when combining conventional MRI+ADC+MRS at long TE (**a**). A more accurate separation was obtained when using conventional MRI+ADC+MRS at short TE (**b**). Combination of MRI+ADC+MRS at long and short TE successfully separated the three groups of lesions (**c**), but this was not really more accurate than using MRI+ADC+MRS at short TE

but not in differentiating different tumor types in the same grade [3]. The only report on GG and DWI found in the literature included adults and children and showed a significantly higher minADC in GGs compared to low- and high-grade astrocytomes [13].

As shown in Table 3, our results demonstrate that DNTs had the lowest rCBF and rCBV values, followed by FCD and GGs which had the highest ones. However, the small number of cases having PWI data tempers these findings, and further investigations in a larger population are needed for confirmation. Compared to normal parenchyma, it has been reported that DNTs had lower rCBV [4] and this is consistent with our findings. Wang et al. [32] explained the lower rCBV values of DNTs by the lack of angiogenesis. However, abnormal permeability was found in our study as well as an increased CBV in one case with a large DNT (patient no. 5). To our knowledge, no perfusion MRI studies on FCD and GGs in children have been reported so far in the literature.

One of the major findings in our study was that GGs had a significantly higher Cho/S ratio at short TE than DNTs. FCD could also be distinguished from GGs by Cr/S and Cho/Cr ratios at long TE. MR spectroscopy has been increasingly used in the evaluation of intractable epilepsy associated with brain tumors during the last years. Some studies [3, 4, 31] have shown that DNTs are characterized by their normal spectra, and no significant differences were detected in NAA/Cho, NAA/Cr, NAA/Cr+Cho, or Cho/Cr ratios between DNTs and normal brain [4]. Significant increase of mI/Cr ratio at short TE was also reported in DNTs compared to normal parenchyma [4]. However, according to our findings, this spectral pattern can be also seen in FCD in addition to DNTs. Most GGs have been shown to display the features of low-grade gliomas with decreased NAA and increased choline peaks [27], while FCD is characterized by an elevated Cho and a minimally decreased NAA [21, 31]. Nonetheless, the decrease in NAA could be related to functional alterations as demonstrated in adult patients with temporal and frontal lobe epilepsy without evidence of brain lesion on MRI [8, 9].

Although many authors tried to characterize FCD, DNTs, and GGs using MRI, no study comparing the three lesions in epilepsy children has been reported so far except one study using ^{18}F-FDG and ^{11}C-methionine PET in which the authors could separate FCD from DNT and GG, but not in distinguishing each group from the others [26].

Conclusion

Preoperative imaging diagnosis of epileptogenic brain tumors in children is important for the determination of

Table 4 Separation of each lesion group from the others: sensibility and specificity of each technique or combination of techniques

Sensibility/specificity	DNT (%)		FCD (%)		GG (%)	
MRI	87.5	88.89	100	100	75	92.31
MRI+ADC	87.5	100	100	100	100	100
MRS (TE = 135 ms)	62.5	66.67	40	83.33	100	92.31
MRS (TE = 30 ms)	75	77.78	60	83.33	75	92.31
MRI+ADC+MRS[a]	100	100	100	100	100	100

[a]Long TE: NAA/S+Cr/S+Cho/S; Short TE: NAA/S+Cr/S+Cho/S +mI/S

treatment strategies and expectation of outcome. Conventional MRI alone is still insufficient to distinguish DNTs, FCD, and GGs in some cases. In this study, combination of conventional MRI, ADC values, and MRS ratios either at long TE or short TE correctly separated DNT, FCD, and GG groups with sensitivity and specificity of 100%. Multimodal MRI and MRS could thus help in patient management and in making surgical decisions. However, further studies with larger population with histologically proven lesions are needed to confirm the present findings.

References

1. Bilginer B, Yalnizoglu D, Soylemezoglu F, Turanli G, Cila A, Topcu M, Akalan N (2009) Surgery for epilepsy in children with dysembryoplastic neuroepithelial tumor: clinical spectrum, seizure outcome, neuroradiology, and pathology. Childs Nerv Syst 25 (4):485–491
2. Bronen RA, Vives KP, Kim JH, Fulbright RK, Spencer SS, Spencer DD (1997) Focal cortical dysplasia of Taylor, balloon cell subtype: MR differentiation from low-grade tumors. AJNR Am J Neuroradiol 18(6):1141–1151
3. Bulakbasi N, Kocaoglu M, Ors F, Tayfun C, Ucoz T (2003) Combination of single-voxel proton MR spectroscopy and apparent diffusion coefficient calculation in the evaluation of common brain tumors. AJNR Am J Neuroradiol 24(2):225–233
4. Bulakbasi N, Kocaoglu M, Sanal TH, Tayfun C (2007) Dysembryoplastic neuroepithelial tumors: proton MR spectroscopy, diffusion and perfusion characteristics. Neuroradiology 49 (10):805–812
5. Daumas-Duport C, Scheithauer BW, Chodkiewicz JP, Laws ER Jr, Vedrenne C (1988) Dysembryoplastic neuroepithelial tumor: a surgically curable tumor of young patients with intractable partial seizures. Report of thirty-nine cases. Neurosurgery 23(5):545–556
6. El Khashab M, Gargan L, Margraf L, Koral K, Nejat F, Swift D, Weprin B, Bowers DC (2009) Predictors of tumor progression among children with gangliogliomas. Clinical article. J Neurosurg Pediatr 3(6):461–466
7. Fernandez C, Girard N, Paz Paredes A, Bouvier-Labit C, Lena G, Figarella-Branger D (2003) The usefulness of MR imaging in the diagnosis of dysembryoplastic neuroepithelial tumor in children: a study of 14 cases. AJNR Am J Neuroradiol 24(5):829–834
8. Guye M, Le Fur Y, Confort-Gouny S, Ranjeva JP, Bartolomei F, Regis J, Raybaud CA, Chauvel P, Cozzone PJ (2002) Metabolic and electrophysiological alterations in subtypes of temporal lobe epilepsy: a combined proton magnetic resonance spectroscopic imaging and depth electrodes study. Epilepsia 43(10):1197–1209
9. Guye M, Ranjeva JP, Le Fur Y, Bartolomei F, Confort-Gouny S, Regis J, Chauvel P, Cozzone PJ (2005) 1H-MRS imaging in intractable frontal lobe epilepsies characterized by depth electrode recording. NeuroImage 26(4):1174–1183
10. Haddad SF, Moore SA, Menezes AH, VanGilder JC (1992) Ganglioglioma: 13 years of experience. Neurosurgery 31(2):171–178
11. Honavar M, Janota I, Polkey CE (1999) Histological heterogeneity of dysembryoplastic neuroepithelial tumour: identification and differential diagnosis in a series of 74 cases. Histopathology 34 (4):342–356
12. Im SH, Chung CK, Cho BK, Wang KC, Yu IK, Song IC, Cheon GJ, Lee DS, Kim NR, Chi JG (2002) Intracranial ganglioglioma: preoperative characteristics and oncologic outcome after surgery. J Neurooncol 59(2):173–183
13. Kikuchi T, Kumabe T, Higano S, Watanabe M, Tominaga T (2009) Minimum apparent diffusion coefficient for the differential diagnosis of ganglioglioma. Neurol Res 31(10):1102–1107
14. Krsek P, Maton B, Jayakar P, Dean P, Korman B, Rey G, Dunoyer C, Pacheco-Jacome E, Morrison G, Ragheb J, Vinters HV, Resnick T, Duchowny M (2009) Incomplete resection of focal cortical dysplasia is the main predictor of poor postsurgical outcome. Neurology 72(3):217–223
15. Lee BC, Schmidt RE, Hatfield GA, Bourgeois B, Park TS (1998) MRI of focal cortical dysplasia. Neuroradiology 40(10):675–683
16. Lee J, Lee BL, Joo EY, Seo DW, Hong SB, Hong SC, Suh YL, Lee M (2009) Dysembryoplastic neuroepithelial tumors in pediatric patients. Brain Dev 31(9):671–681
17. Louis DN, Ohgaki H, Wiestler OD, Cavenee WK, Burger PC, Jouvet A, Scheithauer BW, Kleihues P (2007) The 2007 WHO classification of tumours of the central nervous system. Acta Neuropathol 114(2):97–109
18. Majores M, von Lehe M, Fassunke J, Schramm J, Becker AJ, Simon M (2008) Tumor recurrence and malignant progression of gangliogliomas. Cancer 113(12):3355–3363
19. Minkin K, Klein O, Mancini J, Lena G (2008) Surgical strategies and seizure control in pediatric patients with dysembryoplastic neuroepithelial tumors: a single–institution experience. J Neurosurg Pediatr 1(3):206–210
20. Morris HH, Matkovic Z, Estes ML, Prayson RA, Comair YG, Turnbull J, Najm I, Kotagal P, Wyllie E (1998) Ganglioglioma and intractable epilepsy: clinical and neurophysiologic features and predictors of outcome after surgery. Epilepsia 39(3):307–313
21. Munakata M, Haginoya K, Soga T, Yokoyama H, Noguchi R, Nagasaka T, Murata T, Higano S, Takahashi S, Iinuma K (2003) Metabolic properties of band heterotopia differ from those of other cortical dysplasias: a proton magnetic resonance spectroscopy study. Epilepsia 44(3):366–371
22. Ogiwara H, Nordli DR, DiPatri AJ, Alden TD, Bowman RM, Tomita T (2010) Pediatric epileptogenic gangliogliomas: seizure outcome and surgical results. J Neurosurg Pediatr 5(3):271–276
23. Ostertun B, Wolf HK, Campos MG, Matus C, Solymosi L, Elger CE, Schramm J, Schild HH (1996) Dysembryoplastic neuroepithelial tumors: MR and CT evaluation. AJNR Am J Neuroradiol 17(3):419–430
24. Ozlen F, Gunduz A, Asan Z, Tanriverdi T, Ozkara C, Yeni N, Yalcinkaya C, Ozyurt E, Uzan M (2010) Dysembryoplastic neuroepithelial tumors and gangliogliomas: clinical results of 52 patients. Acta Neurochir (Wien) 152(10):1661–1671
25. Phi JH, Cho BK, Wang KC, Lee JY, Hwang YS, Kim KJ, Chae JH, Kim IO, Park SH, Kim SK (2010) Longitudinal analyses of the surgical outcomes of pediatric epilepsy patients with focal cortical dysplasia. J Neurosurg Pediatr 6(1):49–56
26. Phi JH, Paeng JC, Lee HS, Wang KC, Cho BK, Lee JY, Park SH, Lee J, Lee DS, Kim SK (2010) Evaluation of focal cortical dysplasia and mixed neuronal and glial tumors in pediatric epilepsy patients using 18F-FDG and 11C-methionine pet. J Nucl Med 51(5):728–734
27. Raybaud C, Shroff M, Rutka JT, Chuang SH (2006) Imaging surgical epilepsy in children. Childs Nerv Syst 22(8):786–809
28. Tate AR, Majos C, Moreno A, Howe FA, Griffiths JR, Arus C (2003) Automated classification of short echo time in in vivo 1H brain tumor spectra: a multicenter study. Magn Reson Med 49 (1):29–36

29. Urbach H (2008) MRI of long-term epilepsy-associated tumors. Semin Ultrasound CT MR 29(1):40–46
30. Urbach H, Scheffler B, Heinrichsmeier T, von Oertzen J, Kral T, Wellmer J, Schramm J, Wiestler OD, Blumcke I (2002) Focal cortical dysplasia of Taylor's balloon cell type: a clinicopathological entity with characteristic neuroimaging and histopathological features, and favorable postsurgical outcome. Epilepsia 43(1):33–40
31. Vuori K, Kankaanranta L, Hakkinen AM, Gaily E, Valanne L, Granstrom ML, Joensuu H, Blomstedt G, Paetau A, Lundbom N (2004) Low-grade gliomas and focal cortical developmental malformations: differentiation with proton MR spectroscopy. Radiology 230(3):703–708
32. Wang L, Li KC, Chen L, Lu DH, Zhang GJ, Li YJ (2005) Perfusion MR imaging and proton MR spectroscopy in a case of dysembryoplastic neuroepithelial tumor. Chin Med J (Engl) 118 (13):1134–1136
33. Yagishita A, Arai N, Maehara T, Shimizu H, Tokumaru AM, Oda M (1997) Focal cortical dysplasia: appearance on MR images. Radiology 203(2):553–559
34. Yamasaki F, Kurisu K, Satoh K, Arita K, Sugiyama K, Ohtaki M, Takaba J, Tominaga A, Hanaya R, Yoshioka H, Hama S, Ito Y, Kajiwara Y, Yahara K, Saito T, Thohar MA (2005) Apparent diffusion coefficient of human brain tumors at MR imaging. Radiology 235(3):985–991
35. Yu AH, Chen L, Li YJ, Zhang GJ, Li KC, Wang YP (2009) Dysembryoplastic neuroepithelial tumors: magnetic resonance imaging and magnetic resonance spectroscopy evaluation. Chin Med J (Engl) 122(20):2433–2437
36. Zentner J, Wolf HK, Ostertun B, Hufnagel A, Campos MG, Solymosi L, Schramm J (1994) Gangliogliomas: clinical, radiological, and histopathological findings in 51 patients. J Neurol Neurosurg Psychiatry 57(12):1497–1502